

Frequent loss of heterozygosity in CRISPR-Cas9–edited early human embryos

Gregorio Alanis-Lobato^a, Jasmin Zohren^b, Afshan McCarthy^a, Norah M. E. Fogarty^{a,c}, Nada Kubikova^{d,e}, Emily Hardman^a, Maria Greco^f, Dagan Wells^{d,g}, James M. A. Turner^b, and Kathy K. Niakan^{a,h,1}

^aHuman Embryo and Stem Cell Laboratory, The Francis Crick Institute, NW1 1AT London, United Kingdom; ^bSex Chromosome Biology Laboratory, The Francis Crick Institute, NW1 1AT London, United Kingdom; ^cCentre for Stem Cells and Regenerative Medicine, Guy's Campus, King's College London, SE1 9RT London, United Kingdom; ^dNuffield Department of Women's and Reproductive Health, John Radcliffe Hospital, University of Oxford, OX3 9DU Oxford, United Kingdom; ^eJesus College, University of Oxford, OX1 3DW Oxford, United Kingdom; ^fAncient Genomics Laboratory, The Francis Crick Institute, NW1 1AT London, United Kingdom; ^gJuno Genetics, OX4 4GE Oxford, United Kingdom; and ^hThe Centre for Trophoblast Research, Department of Physiology, Development and Neuroscience, University of Cambridge, CB2 3EG Cambridge, United Kingdom

Edited by Barbara J. Meyer, University of California, Berkeley, CA, and approved October 31, 2020 (received for review June 5, 2020)

CRISPR-Cas9 genome editing is a promising technique for clinical applications, such as the correction of disease-associated alleles in somatic cells. The use of this approach has also been discussed in the context of heritable editing of the human germ line. However, studies assessing gene correction in early human embryos report low efficiency of mutation repair, high rates of mosaicism, and the possibility of unintended editing outcomes that may have pathologic consequences. We developed computational pipelines to assess single-cell genomics and transcriptomics datasets from OCT4 (*POU5F1*) CRISPR-Cas9–targeted and control human preimplantation embryos. This allowed us to evaluate on-target mutations that would be missed by more conventional genotyping techniques. We observed loss of heterozygosity in edited cells that spanned regions beyond the *POU5F1* on-target locus, as well as segmental loss and gain of chromosome 6, on which the *POU5F1* gene is located. Unintended genome editing outcomes were present in ~16% of the human embryo cells analyzed and spanned 4–20 kb. Our observations are consistent with recent findings indicating complexity at on-target sites following CRISPR-Cas9 genome editing. Our work underscores the importance of further basic research to assess the safety of genome editing techniques in human embryos, which will inform debates about the potential clinical use of this technology.

genome editing | CRISPR-Cas9 | human embryo | segmental aneuploidy | loss of heterozygosity

Clustered regularly interspaced short palindromic repeat (CRISPR)–CRISPR associated 9 (Cas9) genome editing is not only an indispensable molecular biology technique (1) but also has enormous therapeutic potential as a tool to correct disease-causing mutations (2). Genome editing of human embryos or germ cells to produce heritable changes has the potential to reduce the burden of genetic disease, and its use in this context is currently a topic of international discussions centered around ethics, safety, and efficiency (3, 4).

Several groups have conducted studies to assess the feasibility of gene correction in early human embryos (5–7), and they all encountered low efficiency of gene repair and high levels of mosaicism (i.e., embryos with corrected as well as mutant uncorrected blastomeres or blastomeres with unintended insertion/deletion mutations), which are unacceptable outcomes for clinical applications. In 2017, Ma et al. set out to correct a 4-bp pathogenic heterozygous deletion in the *MYBPC3* gene using the CRISPR-Cas9 system (8). The experimental strategy involved coinjection of Cas9 protein, a single guide RNA (sgRNA) that specifically targeted the *MYBPC3* mutation and a repair template into either fertilized eggs (zygotes) or oocytes, coincident with intracytoplasmic sperm injection. Analysis of the resulting embryos revealed a higher than expected incidence, with respect to controls, of samples where only WT copies of the gene were detectable (8). Intriguingly, the excess of apparently uniformly

homozygous WT embryos in both cases was not associated with use of the provided repair template for gene correction. Instead, the authors suggest that in edited embryos the WT maternal allele served as a template for the high-fidelity homology directed repair (HDR) pathway to repair the double-strand lesion caused by the Cas9 protein in the paternal allele (8).

Ma and coworkers' interpretation of gene editing by inter-homolog homologous recombination (IH-HR) in the early human embryo has been met with skepticism because alternative explanations can account for the observed results (9–11). One of these is that the CRISPR-Cas9 system can induce large deletions and complex genomic rearrangements with pathogenic potential at the on-target site (9, 10, 12–14). These events can be overlooked because genotyping of the targeted genomic locus often involves the amplification of a small PCR fragment centered around the on-target cut site. CRISPR-Cas9–induced deletions larger than these fragments in either direction would eliminate one or both PCR primer annealing sites. This, in turn, can lead to amplification of only one allele, giving the false impression that targeting was unsuccessful or that there is a single homozygous event at the on-target site (9, 10, 15). Loss of heterozygosity (LOH) can also be the result of more complex genomic rearrangements like inversions, large insertions, translocations, chromosome loss, and even IH-HR with crossover, whereby a large piece of one parental allele is integrated by the other parental chromosome at the on-target cut site (15).

The reported frequencies of unintended CRISPR-Cas9 on-target damage are not negligible. Adikusama et al. targeted six genes in a total of 127 early mouse embryos and detected large deletions (between 100 bp and 2.3 kb) in 45% of their samples using long-range PCR (10). Of note, large deletions were generally more prevalent when they targeted intronic regions (>70%) than

This paper results from the NAS Colloquium of the National Academy of Sciences, "Life 2.0: The Promise and Challenge of a CRISPR Path to a Sustainable Planet," held December 10–11, 2019, at the Arnold and Mabel Beckman Center of the National Academies of Sciences and Engineering in Irvine, CA. NAS colloquia began in 1991 and have been published in PNAS since 1995. The complete program and video recordings of presentations are available on the NAS website at <http://www.nasonline.org/CRISPR>. The collection of colloquium papers in PNAS can be found at <https://www.pnas.org/page/collection/crispr-sustainable-planet>.

Author contributions: G.A.-L., J.Z., J.M.A.T., and K.K.N. designed research; G.A.-L., A.M., N.M.E.F., N.K., E.H., M.G., and D.W. performed research; G.A.-L. and J.Z. contributed new analytic tools; G.A.-L., J.Z., and K.K.N. analyzed data; and G.A.-L. and K.K.N. wrote the paper with input from all authors.

The authors declare no competing interest.

This article is a PNAS Direct Submission.

Published under the PNAS license.

¹To whom correspondence may be addressed. Email: kathy.niakan@crick.ac.uk.

This article contains supporting information online at <https://www.pnas.org/lookup/suppl/doi:10.1073/pnas.2004832117/-DCSupplemental>.

Published April 9, 2021.

when they targeted exons (20%). Consistent with this, Kosicki et al. observed large deletions (up to 6 kb) and other complex genomic lesions at frequencies of 5–20% of their clones after targeting the *PigA* and *Cd9* loci in two mouse embryonic stem cell (mESC) lines and primary mouse cells from the bone marrow, as well as the *PIGA* gene in immortalized human female retinal pigment epithelial cells (12). Moreover, Owens et al. used CRISPR-Cas9 with two sgRNAs to delete 100–150 bp in the *Runx1* locus of mESCs and found that 23% of their clones had large deletions (up to 2 kb) that escaped genotyping by short-range PCR (giving the impression that they were homozygous WT clones), with these complex on-target events becoming evident using long-range PCR (14). Similar damage and frequencies were also observed with the Cas9^{D10A} nickase (14). More dramatic events were identified by Cullot et al., who CRISPR-targeted the *UROS* locus in HEK293T and K562 cells for HDR correction with a repair template (13). Their experiments suggest that CRISPR-Cas9 can induce megabase scale chromosomal truncations (~10% increase compared to controls). However, these cells have abnormal karyotypes and are p53 deficient, which may impact on their DNA damage repair machinery. In fact, they did not see the same effect in human foreskin fibroblasts but knocking out of *TP53* in these primary cells increased the large deletion events by 10-fold (13). More recently, Przewrocka et al. observed a 6% incidence of chromosome arm truncations when targeting *ZNF516* in p53-competent HCT116 cancer cell lines with CRISPR-Cas9, suggesting that *TP53* expression alone may not predict predisposition of cells to large on-target mutations (16).

Our laboratory used CRISPR-Cas9 genome editing to investigate the function of the pluripotency factor OCT4 (encoded by the *POU5F1* gene on the p-arm of chromosome 6) during human preimplantation development (17). We generated a number of single-cell amplified genomic DNA (gDNA) samples for genotyping and confirmed on-target genome editing in all microinjected embryos and a stereotypic insertion/deletion (indel) pattern of mutations with the majority of samples exhibiting a 2-bp deletion (17). However, we noted that in five of the samples analyzed, the genotype could not be determined because of failures to PCR amplify the on-target genomic fragment. This finding suggested complexity at the on-target region that may have abolished one or both PCR primer binding sites. Moreover, we identified that 57 of the 137 successfully genotyped samples (42%) exhibited a homozygous WT genotype based on PCR amplification of a short genomic fragment (17). We originally interpreted these cases as unsuccessful targeting events, however, given the frequencies of the on-target complexities noted above, we speculated that our previous methods may have missed more complex on-target events.

Here, we have developed computational pipelines to analyze single-cell low-pass whole genome sequencing (WGS), transcriptome, and deep-amplicon sequencing data to assess the prevalence of LOH events in the context of CRISPR-Cas9-edited early human embryos. Our results indicate that LOH events on chromosome 6, including chromosomal and segmental copy number abnormalities, are more prevalent in OCT4-edited embryos compared to both Cas9-injected and Cas9-uninjected controls, adding to the growing body of literature reporting that CRISPR-Cas9 genome editing can cause unintended on-target damage. Altogether, this underscores the importance of evaluating genome-edited samples for a diversity of mutations, including large-scale deletions, complex rearrangements, and cytogenetic abnormalities, undetectable with methods that have routinely been used to interrogate targeted sites in previous studies. Our results sound a note of caution for the potential use of the CRISPR-Cas9 genome editing technology described here for reproductive purposes.

Results

Segmental Losses and Gains at a CRISPR-Cas9 On-Target Site Identified by Cytogenetics Analysis. In our previous study (17), in vitro fertilized zygotes donated as surplus to infertility treatment were microinjected with either an sgRNA-Cas9 ribonucleoprotein complex to target *POU5F1* or Cas9 protein alone as a control and cultured for up to 6 d (targeted and control samples, respectively). We collected a single cell or a cluster of 2–5 cells from these embryos for cytogenetic, genotyping, or transcriptomic analysis (*SI Appendix, Fig. S1*).

To determine whether CRISPR-Cas9 genome editing leads to complex on-target DNA damage that would have been missed by our previous targeted amplicon sequencing, we reanalyzed low-pass WGS data following whole-genome amplification (WGA) from 23 OCT4-targeted and 8 Cas9 control samples (*SI Appendix, Table S1*). Given the small sample size, we microinjected additional human embryos with a ribonucleoprotein complex to target *POU5F1*, or the Cas9 enzyme as a control, followed by single-cell WGA and low-pass WGS, as before (17). Here and below, the prefix that distinguishes the processing steps is followed by an embryo number and a cell number. The samples used for low-pass WGS were identified with prefix L_ (*SI Appendix, Fig. S1*). The letter C precedes the embryo number to distinguish CRISPR-Cas9 targeted from control samples (*SI Appendix, Fig. S1*). Low-pass WGS data were used to generate copy number profiles for each sample to investigate the presence of abnormalities with a focus on chromosome 6 (Fig. 1A). As an additional comparison, we performed single-cell WGA and low-pass WGS of uninjected control embryos and distinguish these samples with a letter U preceding the embryo number (*SI Appendix, Fig. S1*).

After preprocessing and quality control, we examined the profiles of 65 samples (25 CRISPR-Cas9 targeted, 16 Cas9 controls, and 24 uninjected controls; *SI Appendix, Fig. S2A and B*). Fifty-six samples exhibited two copies of chromosome 6 with no obvious cytogenetic abnormalities (Fig. 1C and D and *SI Appendix, Figs. S3–S5*). Seventeen of the CRISPR-Cas9-targeted samples, or 68%, had no evidence of abnormalities on chromosome 6. By contrast, we observed that 8 of the 25 targeted samples had evidence of abnormalities on chromosome 6. Four targeted samples presented a segmental loss or gain that was directly adjacent to or within the *POU5F1* locus on the p-arm of chromosome 6 (Fig. 1B and D and *SI Appendix, Fig. S5*). Interestingly, this included two cells from the same embryo where one exhibited a segmental gain and the other a reciprocal loss extending from 6p21.3 to the end of 6p (Fig. 1B). Altogether, segmental abnormalities were detected in 16% of the total number of CRISPR-Cas9-targeted samples that were evaluated. We also observed that four targeted samples had evidence of a whole gain of chromosome 6 (Fig. 1B and D and *SI Appendix, Fig. S5*), which also represents 16% of the targeted samples examined. Conversely, a single Cas9 control sample (6.25%) had evidence of a segmental gain on the q-arm of chromosome 6, which was at a site distinct from the *POU5F1* locus (*SI Appendix, Fig. S4*). The uninjected controls did not display any chromosomal abnormalities (Fig. 1D and *SI Appendix, Fig. S3*).

The number of segmental and whole-chromosome abnormalities observed in the CRISPR-Cas9-targeted human cells was significantly different from that in the Cas9 ($P = 0.0144$, two-tailed Fisher's test) and uninjected control ($P = 0.0040$, two-tailed Fisher's test) samples (Fig. 1D). Moreover, this significant difference can be attributed to the observed segmental abnormalities on 6p, because excluding them from the comparison results in a negligible difference in whole-chromosome abnormalities between targeted and Cas9 control samples ($P = 0.1429$, two-tailed Fisher's test). This conclusion is further supported by the fact that none of the targeted samples show segmental losses or gains on the p-arm of chromosomes 5 and 7, the closest in

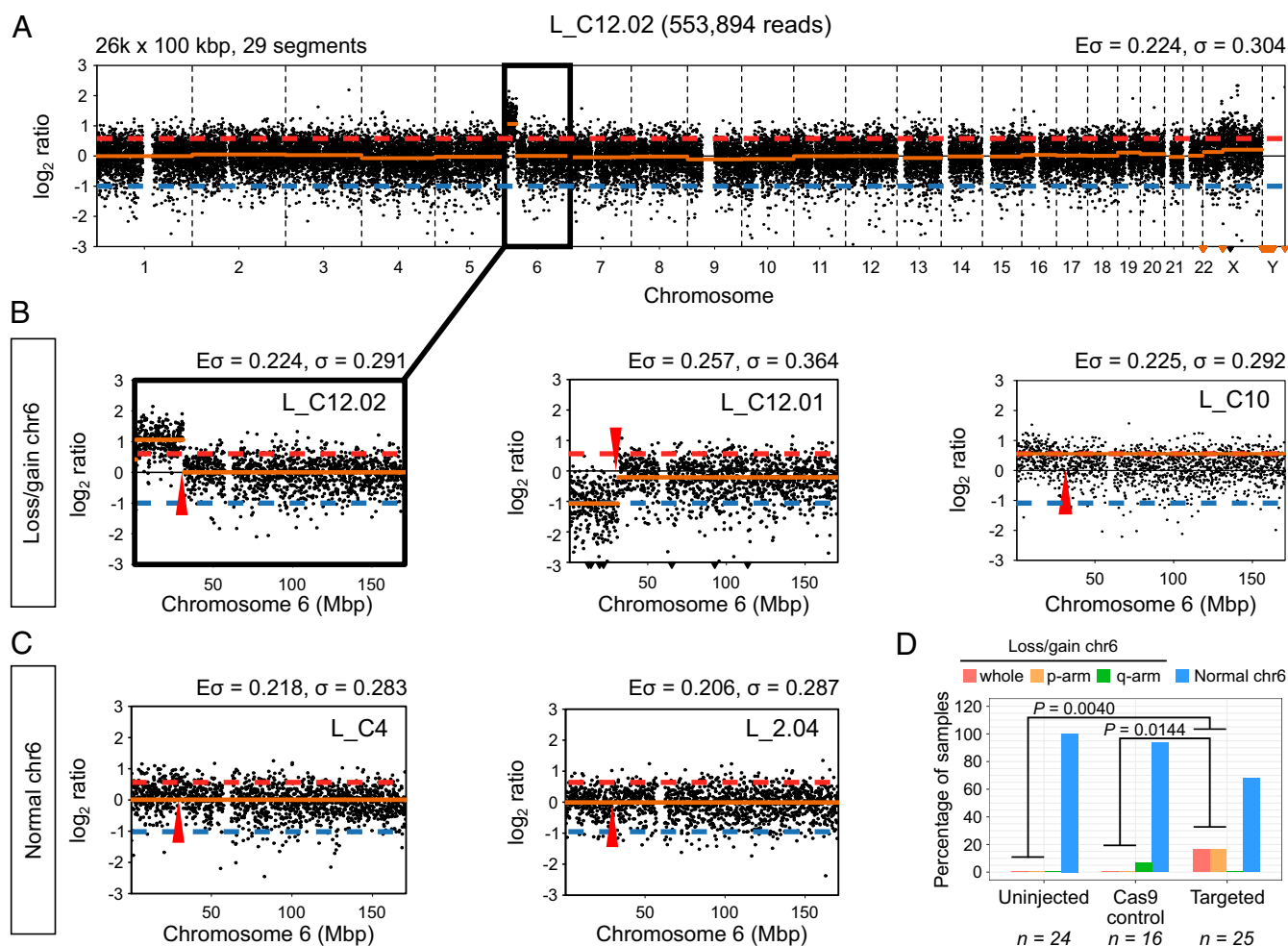


Fig. 1. Segmental losses/gains of chromosome 6 are prevalent in OCT4-targeted embryo samples. (A) Copy number profile of sample L_C12.02. The segmental gain of chromosome 6 is highlighted. The profile was constructed with 26,000 bins of size 100 kbp, which produced 29 segments. The expected ($E\sigma$) and measured (σ) SD of the profile are reported. (B) Zoomed-in view of the copy number profile for samples with segmental losses or gains of chromosome 6. (C) Zoomed-in view of the copy number profile for samples with normal chromosome 6. The $E\sigma$ and σ reported in B and C correspond to the chromosome only. The approximate position of the *POU5F1* gene is indicated by a red arrowhead. The red dashed line indicates a copy ratio of 3:2, while the blue dashed lines corresponds to a copy ratio of 1:2. (D) The percentage of control and targeted samples with whole or segmental losses/gains of chromosome 6 according to their copy number profiles. P values are the result of two-tailed Fisher's tests.

overall size to chromosome 6, but the frequency of whole chromosome abnormalities is similar to that observed for chromosome 6, suggesting that genome editing does not exacerbate the rates of whole chromosome errors (SI Appendix, Fig. S2C). The comparison we performed between Cas9 control and CRISPR-Cas9 genome edited samples includes a combination of both cleavage and blastocyst stage samples (SI Appendix, Table S1). Because rates of aneuploidy are known to be significantly higher at the cleavage stage compared to the blastocyst (18), we wondered whether excluding the samples at the earlier cleavage stage would alter the conclusions drawn about the rates of aneuploidy in CRISPR-Cas9-targeted cells. Here, we found that in comparison to uninjected controls there remained a significantly higher proportion of chromosome 6 aneuploidies in OCT4-targeted cells collected at the blastocyst stage (SI Appendix, Fig. S2D). Altogether, low-pass WGS analysis suggests that a significant proportion of unexpected on-target events leads to segmental abnormalities following CRISPR-Cas9 genome editing in human preimplantation embryos.

LOH Identified by Targeted Deep Sequencing. The copy-number profiles described above with low-pass WGS data can only provide a coarse-grained karyotype analysis. To independently investigate

the prevalence of LOH events at finer resolution and increased sequencing depth, we designed PCR primer pairs to amplify 15 fragments spanning a ~20-kb region containing the *POU5F1* locus. We also included a control PCR amplification in the *ARGFX* locus located on chromosome 3 (SI Appendix, Table S4). The PCR amplicons were used to perform deep sequencing by Illumina MiSeq using the gDNA isolated and amplified from 137 single cells or a cluster of 2–5 microdissected cells (111 CRISPR-Cas9 targeted and 26 Cas9 controls) (SI Appendix, Fig. S1 and Table S2). The prefix W_ distinguished samples whose gDNA was isolated solely for WGA and the prefix G_ was used to demarcate samples that underwent WGA via the genome and transcriptome-sequencing (G&T-seq) protocol (19). All of these samples were different from the samples used for the cytogenetic analyses above.

We then took advantage of the high coverage obtained at each of the sequenced fragments to call single-nucleotide polymorphisms (SNPs), which allowed us to identify samples with putative LOH events: Cases in which heterozygous variants, indicative of contribution from both parental alleles, cannot be confidently called in the amplicons flanking the CRISPR-Cas9 on-target site directly. Since we do not have the parental genotype from any of

the samples that we analyzed, we cannot exclude the possibility that they inherited a homozygous genotype. Therefore, we required the presence of heterozygous SNPs in at least one additional cell from the same embryo to call putative LOH events.

The variant-calling pipeline that we implemented was specifically adjusted for MiSeq data from single cell amplified DNA and includes stringent preprocessing and filtering of the MiSeq reads (*Methods*). To have sufficient depth of coverage and to construct reliable SNP profiles, we only considered samples with $\geq 5\times$ coverage in at least two-thirds of the amplicons across the *POU5F1* locus (*Methods* and *SI Appendix, Fig. S6A*). This threshold allowed us to retain as many samples as possible and still be confident in SNP calling (20). In addition, we implemented a step in our SNP calling pipeline to control for allele

overamplification bias, which is a common issue with single cell-amplified DNA (21). This step changes homozygous calls to heterozygous if the fraction of reads supporting the reference allele is above the median value across samples (*SI Appendix, Fig. S6 B and C* and *Methods*). Thus, we proceeded with 42 CRISPR-Cas9-targeted and 10 Cas9 control samples with reliable SNP profiles for subsequent analysis. These data led to the identification of four different patterns: samples without clear evidence of LOH, samples with LOH at the on-target site, bookended, and open-ended LOH events (Fig. 2A and *SI Appendix, Figs. S7–S12*).

In samples without LOH (20% of control and 11.9% of targeted samples), we were able to call heterozygous SNPs in multiple amplified fragments (G_8.04, G_C16.05, and W_C16.05, Fig. 2A). Cases with putative LOH at the locus have heterozygous SNPs in

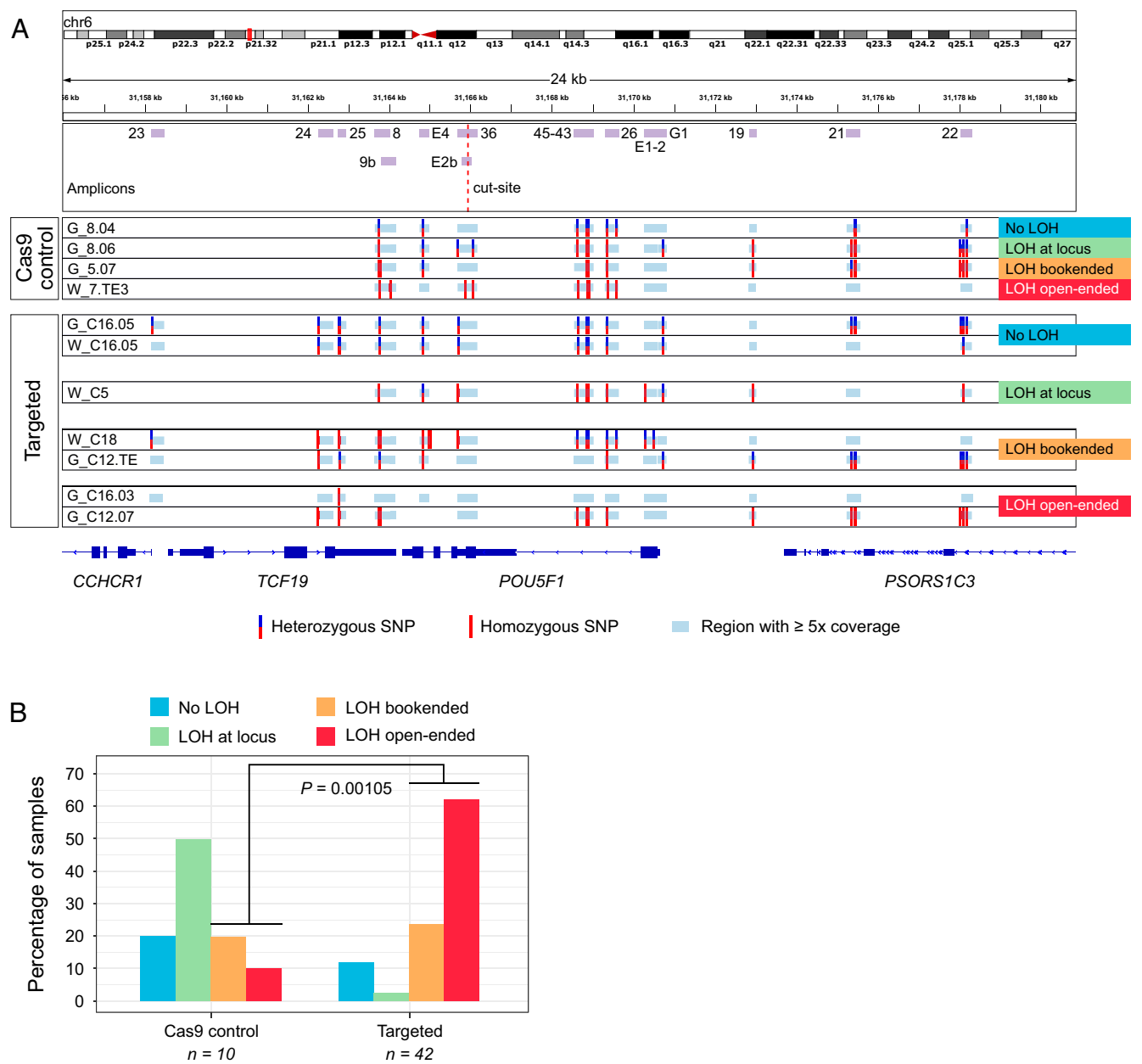


Fig. 2. LOH in the *POU5F1* locus is prevalent among OCT4-targeted embryo samples. (A) SNP profiles constructed from deep sequencing of the depicted amplicons. The four types of LOH events observed are exemplified. Note that there are amplicons with $\geq 5\times$ coverage in which SNPs were not called because all reads agree with the reference genome. (B) The frequency of each type of LOH event in control and targeted samples. P value is the result of a two-tailed Fisher's test.

the amplicons covering exons 1 and 5 of the *POU5F1* gene (fragments E1-2, G1, and E4 in Fig. 2A) and homozygous SNPs in between (50% of control and 2.4% of targeted samples). These putative LOH samples would have had to have a cell isolated from the same embryo that had a detectable SNP(s) anywhere in between these flanking exons (e.g., see samples G_8.03 versus G_8.04 in *SI Appendix, Fig. S7*). Interestingly, this was the most prevalent pattern in Cas9 control samples (Fig. 2B and *SI Appendix, Fig. S7*), which may indicate the possibility of technical issues due to sequencing or overamplification of one parental allele (see below). Bookended samples have two heterozygous SNPs flanking the cut site but in fragments outside the *POU5F1* locus (20% of control and 23.8% of targeted samples). These LOH events could represent deletions of lengths between ~7 kb (G_C12.03, *SI Appendix, Fig. S10*) and ~12 kb (W_C11.04, *SI Appendix, Fig. S9*). Finally, in open-ended samples (10% of control and 61.9% of targeted samples), it was not possible to find heterozygous SNPs in any of the amplified fragments (G_C12.07, Fig. 2A) or there was one or a few heterozygous SNPs on only one side of the region of interest (G_C16.02, *SI Appendix, Fig. S12*). This was the most common pattern in targeted samples (Fig. 2B and *SI Appendix, Figs. S8–S12*) and could represent large deletions of ~20 kb in length (the size of the region explored) or larger.

As mentioned above, the MiSeq data must be interpreted with caution given the presence of LOH in Cas9 controls. The gDNA employed in these experiments was extracted and amplified with a kit based on multiple displacement amplification (MDA, *Methods*), which is common in single-cell applications but is known to have high allelic dropout and preferential amplification rates (22). Although, as mentioned above, we implemented a step to control for these biases, this estimate likely undercalls samples with heterozygosity. For example, some homozygous SNPs had 5% of reads mapping to the reference allele but remained homozygous because they fall below the threshold that we used. Considering that we lack the parental genotypes as a reference to choose a more informed cutoff, our method to calculate one from the data represents an unbiased means to correct the presumed allele overamplification in the samples. Moreover, we cannot exclude the possibility that the analyzed single cells inherited a homozygous genotype in the explored region. Nevertheless, the fact that there is a significant number of CRISPR-Cas9-targeted samples with the largest LOH patterns is notable (Fig. 2B).

Unexpected CRISPR-Cas9-Induced On-Target Events Do Not Lead to Preferential Misexpression of Genes Telomeric to *POU5F1*. Our low-pass WGS and SNP analysis above indicate mutations at the *POU5F1* locus that are larger than discrete indels. We therefore wondered if this on-target complexity may encompass the mutations of genes adjacent or telomeric to *POU5F1* that could complicate the use of CRISPR-Cas9 to understand gene function in human development or other contexts where the analysis of primary cells is required. To address this, we reanalyzed the single-cell RNA sequencing (scRNA-seq) transcriptome datasets (*SI Appendix, Table S6*) we generated previously (17) and focused on the chromosome location of transcripts (Fig. 3A–C). This analysis indicated that differentially expressed genes are not biased to a specific chromosome (Fig. 3A). Moreover, differentially expressed genes are not enriched to either chromosome 6 or the region telomeric to the CRISPR-Cas9 on-target site (Fig. 3D). These results suggest that the transcriptional differences observed as a consequence of *POU5F1* targeting are not confounded by mutations of genes adjacent, or telomeric, to the on-target locus. This could be due to a number of reasons. For example, given that the proportion of samples that exhibit unintended CRISPR-Cas9-induced mutations (e.g., segmental aneuploidies or LOH events) is low, the sample size used is sufficiently high to mask any transcriptional differences in genes adjacent to the cut site in samples with segmental loss of the

p-arm of chromosome 6. It is also possible that the extent of the on-target complexity is exaggerated using the gDNA-based pipelines we developed. Notably, because we use single-cell samples, as mentioned above, these are prone to allele over-amplification and this can confound the interpretation of on-target mutation complexity.

No Evidence of On-Target Complexity Using Digital Karyotype and LOH Analysis of the Single-Cell Transcriptome Data. The use of RNA-sequencing (RNA-seq) data to detect chromosomal abnormalities (23) has great potential to complement the informative low-pass WGS or array CGH methods currently used for embryo screening in the context of assisted reproductive technologies (24, 25). In addition to karyotype analysis, transcriptome data may also provide information about embryo competence at the molecular level. Groff et al. have demonstrated that aneuploidy can be estimated based on significant variations in gene expression in the affected chromosome(s) compared to reference control samples (24). In addition, Weissbein et al. developed a pipeline, called eSNP-Karyotyping, for the detection of LOH in chromosome arms (26). eSNP-Karyotyping is based on measuring the ratio of expressed heterozygous to homozygous SNPs. We applied these two approaches, hereinafter referred to as z-score- and eSNP-Karyotyping, to the scRNA-seq samples (distinguished with the prefix T_) obtained using the G&T-seq protocol (14) (*SI Appendix, Table S3*). This allowed us to investigate whether transcriptome data could be used to determine the frequency of LOH events in CRISPR-Cas9-targeted embryos.

Since eSNP-Karyotyping relies on SNP calls from gene expression data, it is very sensitive to depth and breadth of sequencing (26). Therefore, we used results from this method as a reference to select high quality samples for our transcriptome-based analyses (*SI Appendix, Fig. S13A–C*). After these filtering steps, we retained 38 samples (22 CRISPR-Cas9 targeted and 16 Cas9 controls) to analyze further.

In general, we found good agreement between the chromosomal losses detected by z-score-karyotyping and the LOH events identified by eSNP-Karyotyping (*SI Appendix, Fig. S14A and B*). For example, the digital karyotype of *SI Appendix, Fig. S14A* shows the loss of chromosome 4, the p-arm of chromosome 7, and the q-arm of chromosome 14 in sample T_7.01, as well as the loss of chromosome 3 and the p-arm of chromosome 16 in sample T_C16.06. These abnormalities are identified as LOH events in the eSNP-Karyotyping profiles of the same samples (*SI Appendix, Fig. S14B*). Moreover, the copy number profiles built from low-pass WGS data for different cells from the same embryos also corroborates these chromosomal abnormalities (*SI Appendix, Fig. S13D and E*). In terms of events that could be associated with CRISPR-Cas9 on-target damage, z-score-karyotyping identified the loss of chromosome 6 in sample T_C12.07 (Fig. 4A), which is consistent with the open-ended LOH pattern observed in the gDNA extracted from the same cell G_C12.07 (*SI Appendix, Fig. S10*) and the segmental loss detected in sample L_C12.01 from the same embryo (Fig. 1B). Also, the gain of the p-arm of chromosome 6 was detected in sample T_C12.15 (Fig. 4A), which is consistent with the segmental gain observed in sample L_C12.02 from the same embryo (Fig. 1B). The gains and losses of chromosome 6 in samples T_2.02, T_2.03, T_2.14, T_7.02, and T_C16.06 (Fig. 4A) are difficult to interpret due to the low quality of their MiSeq data or the lack of amplicon information for the q-arm (*SI Appendix, Figs. S7 and S12*). Interestingly, eSNP-Karyotyping did not detect any LOH events in chromosome 6 (*SI Appendix, Fig. S15*), suggesting that this approach is not sensitive enough to detect segmental abnormalities in single-cell samples. Overall, the transcriptome-based karyotypes did not confirm the trends observed in the gDNA-derived data (Fig. 4B).

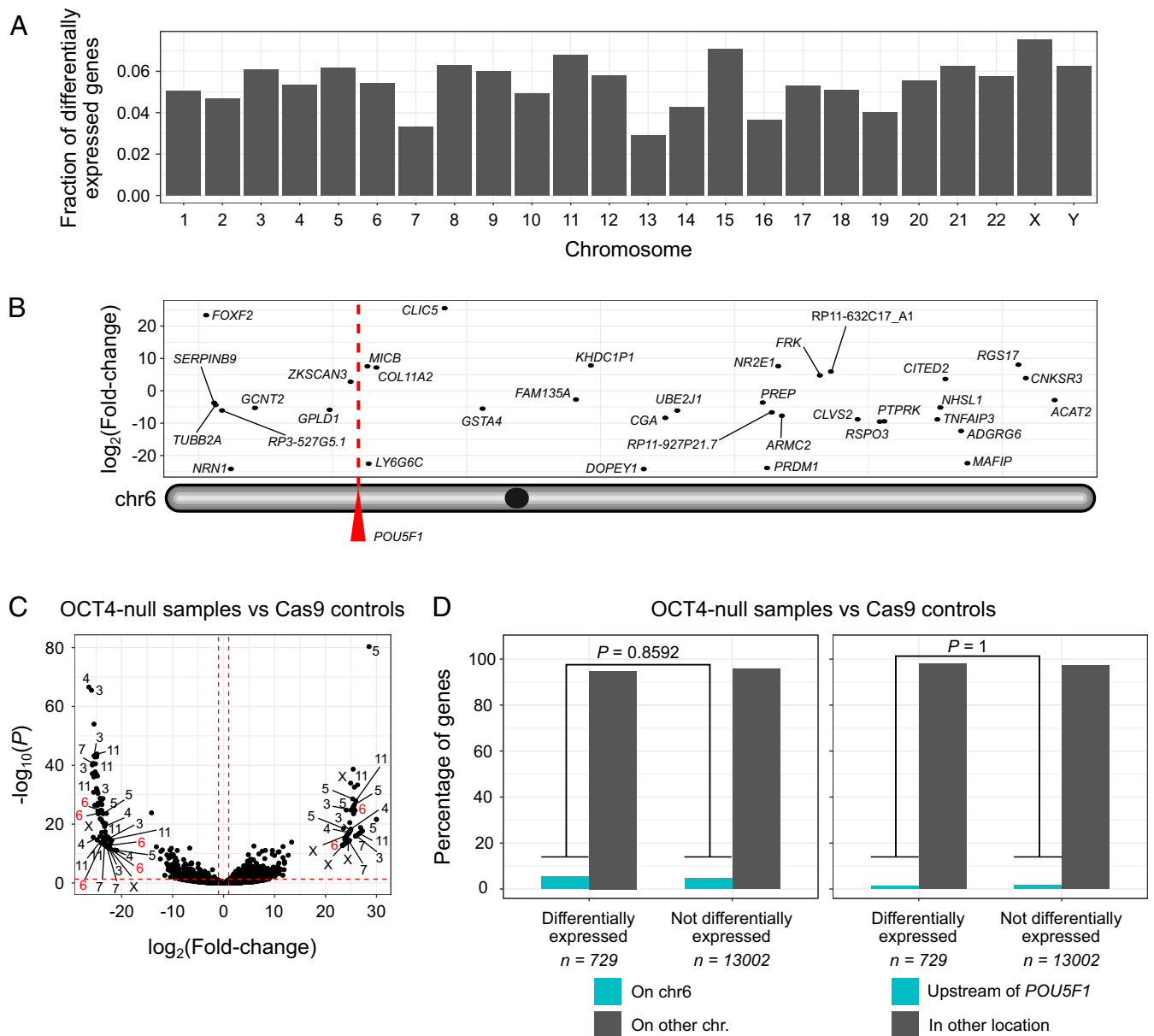


Fig. 3. LOH in OCT4-targeted samples does not lead to preferential misexpression of genes located on chromosome 6. (A) The fraction of differentially expressed genes per chromosome from the comparison between OCT4-null samples and Cas9 controls. (B) Location of differentially expressed genes along chromosome 6. (C) Volcano plot summarizing the comparison between OCT4-null samples and Cas9 controls with differential gene expression analysis. The chromosome location of some of the most dysregulated genes is shown (absolute \log_2 fold change > 20 and Benjamini-Hochberg adjusted $P < 0.05$). The red dashed lines correspond to absolute \log_2 fold changes > 1 and Benjamini-Hochberg adjusted $P < 0.05$. (D) Genes located on chromosome 6 are not over-represented in the list of loci whose expression is disturbed upon OCT4 knock out. The same applies for genes directly upstream to the *POU5F1* gene. P values are the result of two-tailed Fisher's tests.

Discussion

In all, we reveal unexpected on-target complexity following CRISPR-Cas9 genome editing of human embryos. Our data suggest ~16% of samples exhibit segmental losses/gains adjacent to the *POU5F1* locus and LOH events that span 4 kb to at least 20 kb. Chromosome instability, including whole or segmental chromosome gain or loss, is common in human preimplantation embryos (27, 28). However, in contrast to Cas9 control embryos, we noted a significantly higher frequency of CRISPR-Cas9-targeted embryos with a segmental gain or loss that was directly adjacent to the *POU5F1* on-target site. The segmental errors were observed in embryos from distinct genetic backgrounds and donors. Therefore, together with their on-target location, this suggests that the

errors may have been an unintended consequence of CRISPR-Cas9 genome editing. This is supported by the higher frequency of larger LOH events that we observed in CRISPR-Cas9-targeted embryos compared to Cas9 controls using an independent targeted deep-sequencing approach. However, due to the nature of our datasets (shallow sequencing, MDA-amplified gDNA, lack of parental genotypes), we may be overestimating LOH events. This may explain some of the on-target complexity observed in Cas9 control samples but does not account for the significantly higher proportion of LOH in the CRISPR-Cas9-targeted samples. It is important to note that 68% of CRISPR-Cas9-targeted cells did not exhibit any obvious segmental or whole chromosome 6 abnormalities, indicating that their genotype and phenotype, with

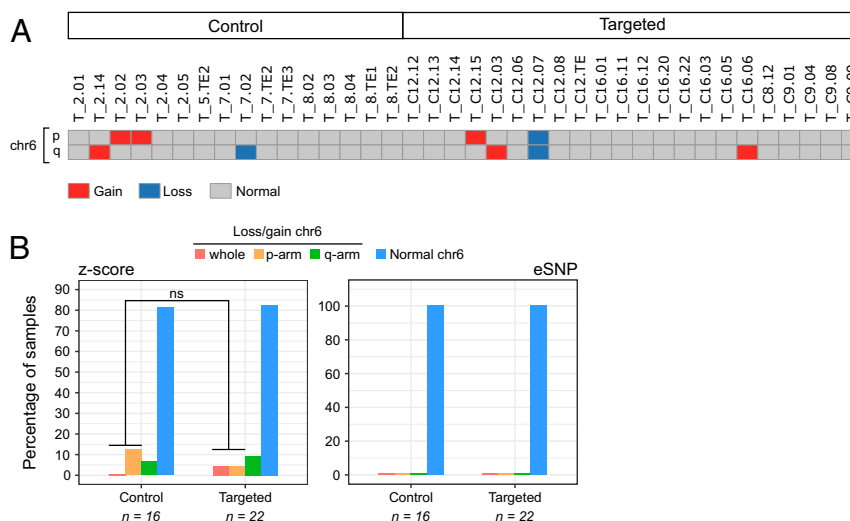


Fig. 4. Transcriptome-based karyotypes do not capture segmental losses/gains of chromosome 6 in OCT4-targeted embryo samples. (A) Digital karyotype based on the total gene expression deviation from the average of each chromosome arm (z-score-karyotyping). Only chromosome 6 is shown (see *SI Appendix, Fig. S14A* for the rest of the chromosomes). (B) The percentage of control and targeted samples with segmental losses/gains of chromosome 6 according to their transcriptome-based karyotype (*SI Appendix, Figs. S14A and S15*). *P* value is the result of a two-tailed Fisher's test.

respect to OCT4 function, are interpretable. Moreover, our transcriptome-based digital karyotypes and differential gene expression analysis indicate biallelic transcripts and gene expression upstream and downstream of the *POU5F1* locus in so far as is resolvable from scRNA-seq data, suggesting that in these samples the LOH does not lead to the misexpression of other genes adjacent to the *POU5F1* locus. Also, our work and previous accounts of unexpected CRISPR-Cas9-editing outcomes (9, 10, 12–14, 16) indicate that the frequency of discrete on-target events predominates, which should increase the confidence of the interpretation of functional studies in human embryos. Given the likelihood of mosaicism, it is unclear whether the segmental abnormalities we observed in any one cell analyzed from each embryo are representative of the entire CRISPR-Cas9-targeted embryo or a subset of cells within the embryo. Altogether, this points to the need to use robust techniques to distinguish cells affected by on-target complexity and large deletions following CRISPR-Cas9-mediated genome editing from cells with less complex mutations and our computational pipelines and multiomics analyses are approaches that may be used in the future.

By contrast, we did not observe significantly more abnormalities on chromosome 6 using methods to determine LOH or karyotype from scRNA-seq datasets. There are several factors that could account for the discrepancy between these datasets. First, we do not have the transcriptome from the same samples that showed gains and losses of chromosome 6 in the cytogenetics analysis. A follow-up study in which both transcriptomics and cytogenetics data are extracted from the same sample would be very informative and could be performed by modifying the G&T-seq protocol (19) to incorporate a multiple annealing and looping-based amplification cycles (MALBAC) method for WGA (29) in place of MDA, which was used here due to the proofreading activity of the phi29 MDA polymerase at the expense of high preferential amplification rates (22). Second, mosaicism is common in human preimplantation embryos (30), and this could explain why the digital karyotypes based on gene expression did not detect abnormalities at the same rate as the copy number profiles. Another possibility is that the LOH events are not sufficiently large to impact total gene expression of chromosome 6, which is what z-score- and eSNP-Karyotyping rely on. This could also account for the cytogenetics results, as LOH up to a few megabases in size could cause mapping issues

due to the very low coverage of shallow sequencing that are reflected as gains and losses of whole chromosome segments. Finally, the LOH events detected by gDNA-derived data may only affect genes that are not expressed in the embryo context or whose expression is so low that it cannot be accurately measured by scRNA-seq. So, when z-score- and eSNP-Karyotyping compare gene or SNP expression of targeted versus control samples, no significant differences are identified.

The segmental aneuploidies identified by cytogenetics analysis (Fig. 1B and *SI Appendix, Figs. S3–S5*) most probably point to the occurrence of complex genomic rearrangements in OCT4-targeted samples, such as chromosomal translocations or end-to-end fusions, as it seems unlikely that the rest of the chromosome would continue to be retained without a telomere (31–33). It is likely that human embryos tolerate aneuploidy up to embryo genome activation, given that even embryos with observed multipolar spindles continue to develop during early cleavage divisions (34). Following this, chromosomal anomalies are likely to become increasingly detrimental to cellular viability, although a degree of tolerance may persist in trophoblast cells (28). Why early embryos fail to arrest despite chaotic chromosomal errors such as multipolar spindle formation or presumptive unresolved double-strand breaks following CRISPR-Cas9 genome editing is unclear and crucial to understand. An important next step to gain insights into the extent of the damage would be to use alternative methods. One possibility to understand the complexity would be to perform cytogenetic analysis using fluorescence in situ hybridization (FISH) (35) to probe for segments of chromosome 6. Another option is a chromosome walk-along approach to amplify genomic fragments even further away from the 20-kb genomic region that we evaluated, in order to bookend heterozygous SNPs on either side of the *POU5F1* on-target site. This may be kilobases or megabases away from the on-target site based on previous publications in the mouse or human cell lines (9, 10, 12–14).

Based on our data, the possibility of gene editing via IH-HR cannot be definitely excluded. A preprint by Liang et al. (36) suggests that IH-HR could be one of the major DNA double-strand break repair pathways in human embryos. Following a similar approach to their previous study (8), the authors used CRISPR-Cas9-mediated genome editing to target a paternal mutation and were able to amplify an ~8-kb genomic DNA fragment which, together with G-banding and FISH of ESCs

derived from targeted embryos, suggests that repair from the maternal chromosome by IH-HR results in a stretch of LOH. Of note, due to the selection bias that occurs during ESC derivation and the mosaicism observed following genome editing, it is not possible to draw definitive conclusions about the extent of LOH or its cause in an embryo context, whereby cells with complex mutations may be preferentially excluded from ESC derivation. By contrast, another study by Zuccaro et al., using the same microinjection method, suggests that the LOH observed following CRISPR-Cas9-mediated genome editing is a consequence of whole chromosome or segmental loss adjacent to the on-target site and that microhomology-mediated end-joining (MMEJ) is the dominant repair pathway in this context (37). This corroborates our previous findings in human embryos targeted postfertilization, where we noted a stereotypic pattern to the type of indel mutations and speculated that this was likely due MMEJ (17). Although microhomologies can promote gene conversion by, for example, interchromosomal template switching in a RAD51-dependent manner (38), based on our previous transcriptome analysis, we found that components of the MMEJ pathway (i.e., *POLQ*) are transcribed in early human embryos, while factors essential for HDR (i.e., *RAD51*) are not appreciably expressed. This suggests that MMEJ-derived large deletions (14, 37) are more likely than microhomology-mediated gene conversion in this context, although protein expression has yet to be fully characterized. Consistent with this, a significant fraction of somatic structural variants arises from MMEJ in human cancer (39). Moreover, microhomology-mediated break-induced replication underlies copy number variation in mammalian cells (40) and microhomology/microsatellite-induced replication leads to segmental anomalies in budding yeast (41). The discrepancy between the Liang et al. and Zuccaro et al. studies could be due to locus-dependent differences of CRISPR-Cas9 genome editing fidelity. For example, Przewrocka et al. demonstrate that the proximity of the CRISPR-Cas9-targeted locus to the telomere significantly increases the possibility of inadvertent chromosome arm truncation (16). To fully elucidate the LOH that has occurred at the on-target site in our study, and to resolve the controversy over the IH-HR reported by others (8, 9, 36, 37), will require the development of a pipeline to enrich for the region of interest and then perform deep (long-read) sequencing to evaluate the presence and extent of on-target damage. By bookending SNPs on either side of an LOH event, primers could be designed to incorporate the SNPs and ensure that both parental alleles are amplified. However, this is difficult to perform, and alternative methods include using CRISPR gRNAs to cut just outside of the LOH region followed by long-read sequencing (42).

It would also be of interest to evaluate whether other genome editing strategies, such as prime and base editing, nickases, or improvements in the efficiency of integrating a repair template, may reduce the on-target complexities observed by us and others using spCas9. However, nonnegligible frequencies of editing-associated large deletions have been reported after the use of the Cas9^{D10A} nickase in mESCs (14) and prime editing in early mouse embryos (43). By contrast, while proof-of-principle studies suggest that base editors could be used to repair disease-associated mutations in human embryos, further refinements to reduce the likelihood of unexpected conversion patterns and high rates of off-target edits would be of benefit (2). There are too few studies to date using repair templates. Of the studies that have been conducted, the reported efficiencies of repair with templates in human embryos are very low (5, 7, 8). Modulation of DNA damage repair factors or tethering Cas9 enzymes with a repair template may yield improvements that could allow for the control of editing outcomes.

Our reevaluation of on-target mutations, together with previous accounts of unexpected CRISPR-Cas9 on-target damage (9,

10, 12–14), strongly underscores the importance of further basic research in a number of cellular contexts to resolve the damage that occurs following genome editing. Moreover, this stresses the significance of ensuring whether one or both parental chromosome copies are represented when determining the genotype of any sample to understand the complexity of on-target CRISPR mutations, especially in human primary cells.

Methods

Ethics Statement. We reprocessed the DNA and reanalyzed the data generated in our previous study (17). This corresponds to 168 samples (134 OCT4-targeted and 34 Cas9 controls) across 32 early human embryos (24 OCT4-targeted and 8 Cas9 controls). For the present work, we used 56 additional single-cell samples (19 OCT4-targeted, 12 Cas9 controls, and 25 uninjected controls) across 22 early human embryos (1 OCT4-targeted, 1 Cas9 control, and 20 uninjected controls). This study was approved by the UK Human Fertilization and Embryology Authority (HFEA) (research license no. R0162) and the Health Research Authority's Research Ethics Committee (Cambridge Central reference no. 19/EE/0297). Our research is compliant with the HFEA code of practice and has undergone inspections by the HFEA since the license was granted. Before giving consent, donors were provided with all of the necessary information about the research project, an opportunity to receive counseling, and the conditions that apply within the license and the HFEA Code of Practice. Specifically, patients signed a consent form authorizing the use of their embryos for research including genetic tests and for the results of these studies to be published in scientific journals. No financial inducements were offered for donation. Patient information sheets and the consent documents provided to patients are publicly available (<https://www.crick.ac.uk/research/labs/kathy-niakan/human-embryo-genome-editing-licence>). Embryos surplus to the in vitro fertilization treatment of the patient were donated, cryopreserved, and transferred to the Francis Crick Institute, where they were thawed and used in the research project.

CRISPR-Cas9 Targeting of *POU5F1*. We analyzed single cells or trophectoderm biopsies from human preimplantation embryos that were CRISPR-Cas9 edited in our previous study (17) plus an additional 56 samples used in the present work. In vitro fertilized zygotes donated as surplus to infertility treatment were microinjected with either a sgRNA-Cas9 ribonucleoprotein complex or with Cas9 protein alone and cultured for 5–6 d (targeted and control samples, respectively). The sgRNA was designed to target exon 2 of the *POU5F1* gene, and experiments were performed as previously described (17). Genomic DNA from Cas9 control and OCT4-targeted samples was isolated using the REPLI-g Single Cell Kit (QIAGEN, 150343). DNA samples isolated for cytogenetic analysis were amplified with the SurePlex Kit (Rubicon Genomics). See *SI Appendix* for more details.

Cytogenetic Analysis. Low-pass whole genome sequencing (depth of sequencing <0.1x) libraries were prepared using the VeriSeq PGS Kit (Illumina) or the NEB Ultra II FS Kit and sequenced with the MiSeq platform as previously described (17) or with Illumina HiSeq 4000, respectively. Reads were aligned to the human genome hg19 using BWA v0.7.17 (44) and the copy number profiles generated with QDNaseq v1.24.0 (45). See *SI Appendix* for more details.

PCR Primer Design and Testing. PCR primer pairs were designed with the Primer3 webtool (<https://bioinfo.ut.ee/primer3/>, *SI Appendix, Table S4*). We restricted the product size to 150–500 bp and used the following primer temperature settings: Min = 56, Opt = 58, Max = 60. We tested all primers using 1 µL of genomic DNA from H9 human ES cells in a PCR containing 12.5 µL of Phusion High Fidelity PCR Master Mix (NEB, M0531L), 1.25 µL of 5 µM forward primer, 1.25 µL of 5 µM reverse primer, and 9 µL of nuclease-free water. Thermocycling settings were: 95 °C at 5 min, 35 cycles of 95 °C at 30 s, 58 °C at 30 s, 72 °C at 1 min, and a final extension of 72 °C at 5 min. We confirmed the size of the PCR products by gel electrophoresis. See *SI Appendix* for more details.

PCR Amplification and Targeted Deep Sequencing. Isolated DNA was diluted 1:100 in nuclease-free water. We used the QIAgility robot (QIAGEN, 9001531) for master mix preparation (see above) and distribution to 96-well plates (*SI Appendix, Table S5*). Then, the Biomek FX liquid handling robot (Beckman Coulter, 717013) was used to transfer 1 µL of DNA to the master mix plates and to mix the reagents. The PCR was run with the settings described above. PCR products were cleaned with the Biomek FX robot using the chemagic SEQ Pure20 Kit (PerkinElmer, CMG-458). Clean PCR amplicons

from the same DNA sample were pooled to generate 137 libraries that were sequenced by Illumina MiSeq v3. See *SI Appendix* for more details.

SNP Typing. We trimmed the MiSeq paired-end reads with DADA2 (46), corrected substitution errors in the trimmed reads with RACER (47), and mapped the corrected reads to the human genome hg38 with BWA v0.7.17 (44). Subsequently, SAM files were converted to the BAM format and postprocessed using Samtools v1.3.1 (48). SNP calling was performed with BCFtools v1.8 (49) using mpileup and call. SNPs supported by less than 10 reads and with mapping quality below 50 were filtered out. To control for allele overamplification, homozygous SNPs were changed to heterozygous if the fraction of reads supporting the reference allele was at least 6% of the total (21). This threshold corresponds to the median of the distribution of the fraction of reads supporting the reference allele across samples. See *SI Appendix* for more details.

scRNA-Seq Data Analysis. scRNA-seq reads from G&T-seq samples were processed as previously described (17). Samples with a breadth of sequencing below 0.05 were not considered for any downstream analysis (*SI Appendix*, Fig. S13 A–C). Differential gene expression analysis was carried out with DESeq2 v1.10.1 (50). For digital karyotyping based on gene expression, we adapted the method described in ref. 24 to identify gains or losses of chromosomal arms (z-score-karyotyping). For digital karyotyping based on SNP expression, we applied the eSNP-Karyotyping pipeline with default parameters (26). See *SI Appendix* for more details.

1. M. Adli, The CRISPR tool kit for genome editing and beyond. *Nat. Commun.* **9**, 1911 (2018).
2. R. A. Lea, K. K. Niakan, Human germline genome editing. *Nat. Cell Biol.* **21**, 1479–1489 (2019).
3. National Academy of Medicine, National Academy of Sciences, The Royal Society, *Heritable Human Genome Editing* (The National Academies Press, 2020).
4. Nuffield Council on Bioethics, *Genome Editing and Human Reproduction: Social and Ethical Issues* (Nuffield Council on Bioethics, 2018).
5. P. Liang et al., CRISPR/Cas9-mediated gene editing in human triploid zygotes. *Protein Cell* **6**, 363–372 (2015).
6. X. Kang et al., Introducing precise genetic modifications into human 3PN embryos by CRISPR/Cas-mediated genome editing. *J. Assist. Reprod. Genet.* **33**, 581–588 (2016).
7. L. Tang et al., CRISPR/Cas9-mediated gene editing in human zygotes using Cas9 protein. *Mol. Genet. Genomics* **292**, 525–533 (2017).
8. H. Ma et al., Correction of a pathogenic gene mutation in human embryos. *Nature* **548**, 413–419 (2017).
9. D. Egli et al., Inter-homologue repair in fertilized human eggs? *Nature* **560**, E5–E7 (2018).
10. F. Adikusuma et al., Large deletions induced by Cas9 cleavage. *Nature* **560**, E8–E9 (2018).
11. H. Ma et al., Ma et al. reply. *Nature* **560**, E10–E23 (2018).
12. M. Kosicki, K. Tomberg, A. Bradley, Repair of double-strand breaks induced by CRISPR-Cas9 leads to large deletions and complex rearrangements. *Nat. Biotechnol.* **36**, 765–771 (2018).
13. G. Cullot et al., CRISPR-Cas9 genome editing induces megabase-scale chromosomal truncations. *Nat. Commun.* **10**, 1136 (2019).
14. D. D. G. Owens et al., Microhomologies are prevalent at Cas9-induced larger deletions. *Nucleic Acids Res.* **47**, 7402–7417 (2019).
15. H. Lee, J.-S. Kim, Unexpected CRISPR on-target effects. *Nat. Biotechnol.* **36**, 703–704 (2018).
16. J. Przewrocka, A. Rowan, R. Rosenthal, N. Kanu, C. Swanton, Unintended on-target chromosomal instability following CRISPR/Cas9 single gene targeting. *Ann. Oncol.* **31**, 1270–1273 (2020).
17. N. M. E. Fogarty et al., Genome editing reveals a role for OCT4 in human embryogenesis. *Nature* **550**, 67–73 (2017).
18. E. Fragouli, S. Alfarawati, K. Spath, D. Wells, Morphological and cytogenetic assessment of cleavage and blastocyst stage embryos. *Mol. Hum. Reprod.* **20**, 117–126 (2014).
19. I. C. Macaulay et al., G&T-seq: Parallel sequencing of single-cell genomes and transcriptomes. *Nat. Methods* **12**, 519–522 (2015).
20. T. Kishikawa et al., Empirical evaluation of variant calling accuracy using ultra-deep whole-genome sequencing data. *Sci. Rep.* **9**, 1784 (2019).
21. N. Kubikova et al., Clinical application of a protocol based on universal next-generation sequencing for the diagnosis of beta-thalassaemia and sickle cell anaemia in preimplantation embryos. *Reprod. Biomed. Online* **37**, 136–144 (2018).
22. E. Borgström, M. Paterlini, J. E. Mold, J. Frisen, J. Lundberg, Comparison of whole genome amplification techniques for human single cell exome sequencing. *PLoS One* **12**, e0171566 (2017).
23. J. A. Griffiths, A. Scialdone, J. C. Marioni, Mosaic autosomal aneuploidies are detectable from single-cell RNAseq data. *BMC Genomics* **18**, 904 (2017).
24. A. F. Groff et al., RNA-seq as a tool for evaluating human embryo competence. *Genome Res.* **29**, 1705–1718 (2019).
25. M. Poli et al., Past, present, and future strategies for enhanced assessment of embryo's genome and reproductive competence in women of advanced reproductive age. *Front. Endocrinol. (Lausanne)* **10**, 154 (2019).
26. U. Weissbein, M. Schachter, D. Egli, N. Benvenisty, Analysis of chromosomal aberrations and recombination by allelic bias in RNA-Seq. *Nat. Commun.* **7**, 12144 (2016).
27. E. Vanneste et al., Chromosome instability is common in human cleavage-stage embryos. *Nat. Med.* **15**, 577–583 (2009).
28. D. Babariya, E. Fragouli, S. Alfarawati, K. Spath, D. Wells, The incidence and origin of segmental aneuploidy in human oocytes and preimplantation embryos. *Hum. Reprod.* **32**, 2549–2560 (2017).
29. C. Zong, S. Lu, A. R. Chapman, X. S. Xie, Genome-wide detection of single-nucleotide and copy-number variations of a single human cell. *Science* **338**, 1622–1626 (2012).
30. R. C. McCoy, Mosaicism in preimplantation human embryos: When chromosomal abnormalities are the norm. *Trends Genet.* **33**, 448–463 (2017).
31. B. van Steensel, A. Smogorzewska, T. de Lange, TRF2 protects human telomeres from end-to-end fusions. *Cell* **92**, 401–413 (1998).
32. A. W. I. Lo et al., Chromosome instability as a result of double-strand breaks near telomeres in mouse embryonic stem cells. *Mol. Cell Biol.* **22**, 4836–4850 (2002).
33. R. Capper et al., The nature of telomere fusion and a definition of the critical telomere length in human cells. *Genes Dev.* **21**, 2495–2508 (2007).
34. E. Fragouli et al., The origin and impact of embryonic aneuploidy. *Hum. Genet.* **132**, 1001–1013 (2013).
35. E. Fragouli et al., Cytogenetic analysis of human blastocysts with the use of FISH, CGH and aCGH: Scientific data and technical evaluation. *Hum. Reprod.* **26**, 480–490 (2011).
36. D. Liang et al., Frequent gene conversion in human embryos induced by double strand breaks. *bioRxiv*:2020.06.19.162214 (20 June 2020).
37. M. V. Zuccaro et al., Allele-specific chromosome removal after Cas9 cleavage in human embryos. *Cell*, 10.1016/j.cell.2020.10.025 (2020).
38. O. Tsaponina, J. E. Haber, Frequent interchromosomal template switches during gene conversion in *S. cerevisiae*. *Mol. Cell* **55**, 615–625 (2014).
39. Y. Li et al., PCAWG Structural Variation Working Group; PCAWG Consortium, Patterns of somatic structural variation in human cancer genomes. *Nature* **578**, 112–121 (2020).
40. P. J. Hastings, G. Ira, J. R. Lupski, A microhomology-mediated break-induced replication model for the origin of human copy number variation. *PLoS Genet.* **5**, e1000327 (2009).
41. C. Payen, R. Koszul, B. Dujon, G. Fischer, Segmental duplications arise from Pol32-dependent repair of broken forks through two alternative replication-based mechanisms. *PLoS Genet.* **4**, e1000175 (2008).
42. T. Gilpatrick et al., Targeted nanopore sequencing with Cas9-guided adapter ligation. *Nat. Biotechnol.* **38**, 433–438 (2020).
43. T. Aida et al., Prime editing primarily induces undesired outcomes in mice. *bioRxiv*: 020.08.06.239723 (6 August 2020).
44. H. Li, R. Durbin, Fast and accurate long-read alignment with Burrows-Wheeler transform. *Bioinformatics* **26**, 589–595 (2010).
45. I. Scheinin et al., DNA copy number analysis of fresh and formalin-fixed specimens by shallow whole-genome sequencing with identification and exclusion of problematic regions in the genome assembly. *Genome Res.* **24**, 2022–2032 (2014).
46. B. J. Callahan et al., DADA2: High-resolution sample inference from Illumina amplicon data. *Nat. Methods* **13**, 581–583 (2016).
47. L. Ilie, M. Molnar, RACER: Rapid and accurate correction of errors in reads. *Bioinformatics* **29**, 2490–2493 (2013).
48. H. Li et al., 1000 Genome Project Data Processing Subgroup, The sequence alignment/map format and SAMtools. *Bioinformatics* **25**, 2078–2079 (2009).
49. H. Li, A statistical framework for SNP calling, mutation discovery, association mapping and population genetic parameter estimation from sequencing data. *Bioinformatics* **27**, 2987–2993 (2011).
50. M. I. Love, W. Huber, S. Anders, Moderated estimation of fold change and dispersion for RNA-seq data with DESeq2. *Genome Biol.* **15**, 550 (2014).
51. G. Alanis-Lobato et al., Frequent loss-of-heterozygosity in CRISPR-Cas9-edited early human embryos. Sequence Read Archive. <https://www.ncbi.nlm.nih.gov/bioproject/?term=PRJNA637030>. Deposited 3 June 2020.
52. N. M. Fogarty et al., Uncovering mechanisms of early human lineage specification by CRISPR/Cas9-mediated genome editing [RNA-seq]. *Gene Expression Omnibus*. <https://www.ncbi.nlm.nih.gov/geo/query/acc.cgi?acc=GSE100118>. Accessed 10 September 2020.
53. G. Alanis-Lobato et al., Frequent loss-of-heterozygosity in CRISPR-Cas9-edited early human embryos. GitHub. https://github.com/galanis/loh_scripts. Deposited 31 May 2020.